The Annals of Applied Statistics
2016, Vol. 10, No. 1, 477–505
DOI: 10.1214/16-AOAS903

TEMPERATURES IN TRANSIENT CLIMATES: IMPROVED METHODS FOR SIMULATIONS WITH EVOLVING TEMPORAL COVARIANCES[1]

BY ANDREW POPPICK*, DAVID J. MCINERNEY†, ELISABETH J. MOYER* AND MICHAEL L. STEIN*

*University of Chicago** *and University of Adelaide*†

Future climate change impacts depend on temperatures not only through changes in their means but also through changes in their variability. General circulation models (GCMs) predict changes in both means and variability; however, GCM output should not be used directly as simulations for impacts assessments because GCMs do not fully reproduce present-day temperature distributions. This paper addresses an ensuing need for simulations of future temperatures that combine both the observational record and GCM projections of changes in means and temporal covariances. Our perspective is that such simulations should be based on transforming observations to account for GCM projected changes, in contrast to methods that transform GCM output to account for discrepancies with observations. Our methodology is designed for simulating transient (nonstationary) climates, which are evolving in response to changes in CO_2 concentrations (as is the Earth at present). This work builds on previously described methods for simulating equilibrium (stationary) climates. Since the proposed simulation relies on GCM projected changes in covariance, we describe a statistical model for the evolution of temporal covariances in a GCM under future forcing scenarios, and apply this model to an ensemble of runs from one GCM, CCSM3. We find that, at least in CCSM3, changes in the local covariance structure can be explained as a function of the regional mean change in temperature and the rate of change of warming. This feature means that the statistical model can be used to emulate the evolving covariance structure of GCM temperatures under scenarios for which the GCM has not been run. When combined with an emulator for mean temperature, our methodology can simulate evolving temperatures under such scenarios, in a way that accounts for projections of changes while still retaining fidelity with the observational record. The emulator for variability changes is also of interest on its own as a summary of GCM projections of variability changes.

Received July 2015; revised January 2016.

[1]Supported in part by STATMOS, the Research Network for Statistical Methods for Atmospheric and Oceanic Sciences (NSF-DMS awards 1106862, 1106974 and 1107046), and RDCEP, the University of Chicago Center for Robust Decision Making in Climate and Energy Policy (NSF Grant SES-0951576).

Key words and phrases. Climate change, climate variability, transient climate, observation-driven simulation, nonstationary processes, evolutionary spectrum.

1. Introduction. Assessing the potential impacts of future climate change on areas of societal interest, such as agriculture and public heath, requires an understanding of how climate features important to those areas are expected to change. Impacts often depend on more than just the response of global or even local mean temperatures to greenhouse gas forcing. Many agricultural crops, for example, are highly sensitive to even brief periods of stress temperatures, particularly at certain times of the growing cycle, so crop yields can be strongly affected by changes in temperature variability even in the absence of a change in mean [e.g., Wheeler et al. (2000)]. In part because of examples like this, the climate and impacts communities have been interested in understanding changes in temperature variability in future climates.

Potential future changes in temperature variability are not yet well understood. By its third assessment report, the Intergovernmental Panel on Climate Change (IPCC) stated that there was some empirical evidence for a decrease in variability at intra-annual timescales, but sparse evidence for changes in inter-annual variability [IPCC (2001)]. More recent studies have not produced more definitive conclusions, with results apparently depending on specific definitions of variability and timescale as well as on the region being studied [IPCC (2007)]. [The most recent report, IPCC (2013), frames variability changes in the context of extreme events, which are not a subject of this work.] One example of a physical mechanism that might explain variability changes at intra-annual timescales in a particular region is that changes in the polar jet stream can produce more persistent weather patterns over, for example, North America [e.g., Francis and Vavrus (2012)], but the mechanism and even detection of these changes remains controversial [Barnes (2013), Screen and Simmonds (2013)]. Implicit in the broader discussion about variability is that variability changes can differ by timescale of variation or geographic location. Because specific impacts will depend on timescale and geographic location, methods for assessing changes should be able to make such distinctions. That is, understanding projected changes in variability relevant to impacts is a problem of understanding the changes in covariance structure of a spatial-temporal field that is evolving in time.

Beyond empirical studies, the primary tools used to understand and project changes in the distribution of climate variables are atmosphere-ocean general circulation models (GCMs). GCMs are deterministic, physical models that are used to generate runs of modeled climate under, for example, varying forcing scenarios. While GCMs are deterministic, the climate system being modeled is chaotic and so GCM realizations under the same forcing scenario but with different initial conditions will behave as if they were statistically independent. Summarizing the statistical properties of GCM predictions under different forcing scenarios is a challenge on its own.

That said, GCM runs alone are often not sufficient as inputs for impacts assessments, which may require realistic simulations from the full distribution of the Earth's temperatures. It is well understood that GCMs somewhat misrepresent

observed temperature distributions under present conditions: regional mean temperatures may differ from observations by several degrees, and studies have noted discrepancies between higher order moments of the modeled and observed climate distributions [IPCC (2013) and references therein]. On the other hand, GCMs are assumed to produce informative projections of, for example, future changes in mean temperatures due to changes in greenhouse gas forcing: the underlying physics are relatively realistic, and GCMs are able to reproduce observed temperature trends in historical forcing runs [e.g., IPCC (2013)]. Projections of variability changes also have many consistent features across different GCMs, although current studies do not address changes in full covariance structures [e.g., Holmes et al. (2015), Schneider, Bischoff and Płotka (2015)]. Impacts assessments researchers have therefore recognized a need to understand not only how temperature distributions are changing in GCM runs, but also how to combine those projections with the observational record to produce simulations of temperatures that more likely follow the distribution of real future temperatures.

There are two popular classes of approaches for generating such simulations: those that modify GCM output to account for model-observation discrepancies (model-driven procedures), and those that modify observational data to account for changes projected by GCMs (observation-driven procedures); see, for example, Ho et al. (2012) and Hawkins et al. (2013) for reviews of common strategies. The most basic model-driven procedure is simple "bias correction," where the difference in mean between observed temperatures and those in historical GCM runs is estimated and then this estimated bias is subtracted from future GCM runs, assuming it remains constant over time. The most basic observation-driven procedure is the Delta method,[2] where, by contrast, changes in mean temperature are estimated by comparing GCM future runs with those under historical forcing, and this trend is then added to the observational data. Both approaches implicitly assume that GCMs correctly capture changes in mean temperature, but they can result in temperature simulations that have very different higher-order characteristics.

An appealing property of observation-driven procedures like the Delta method is that they preserve attributes of the observations that are not explicitly accounted for in the simulation procedure, a property not shared by model-driven procedures. Figure 1, top row, provides a cartoon illustration of this difference between the two approaches. Here, the cartoon model predicts changes in mean but badly misrepresents the mean and covariance structure of the observations. In such a setting, simple bias correction will maintain the model's misrepresented covariance structure, while the Delta method yields a more realistic simulation [see Hawkins et al. (2013) for a less idealized example]. More complicated versions of bias correction exist that attempt to correct for higher-order discrepancies between models and

[2]The meaning of the term "Delta method" in the geosciences, and in this work, is distinct from its typical use in the statistics literature for methods that employ Taylor expansions to derive asymptotic approximations of properties of functions of random variables.

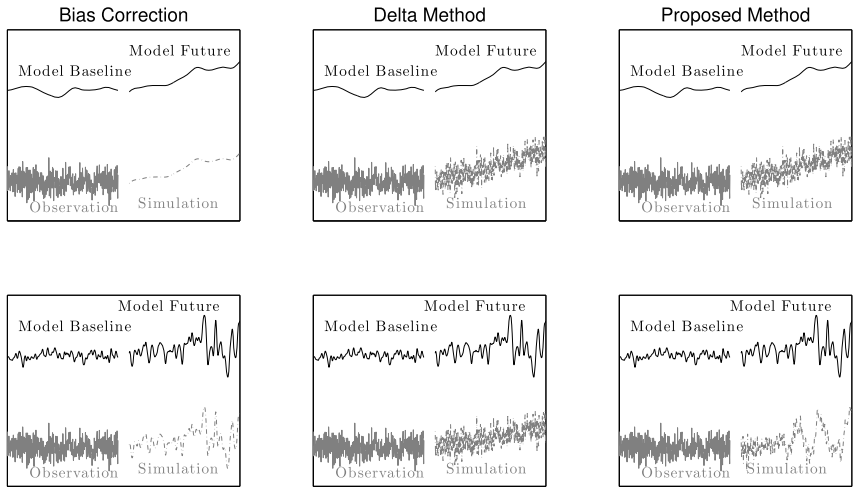

FIG. 1. *Cartoon illustration comparing strategies for simulating temperatures that combine information from a model and the observational record. Columns compare simple bias correction* (*left*), *the Delta method* (*center*) *and our proposed method* (*right*). *Top row, the model predicts changes in mean temperature but no changes in variability*; *in this case, our proposed method is equivalent to the Delta method. Bottom row, the model predicts changes in both mean and covariance. Simple bias correction does not retain the higher order properties of the observations, whereas the Delta method does not account for model changes in covariance*; *our proposed method does both.*

observations. Some correct for discrepancies in marginal distributions [e.g., Wood et al. (2004)], while others additionally attempt to correct rank correlation structures and inter-variable dependence structures [e.g., Piani and Haerter (2012), Vrac and Friederichs (2015)]. While such methods are more sophisticated than the simple bias correction illustrated in Figure 1, they too will leave intact discrepancies between the model and observations not accounted for in the correction procedure. If impacts assessments require realistic simulations from the joint distribution of temperatures across space and time, our perspective is that this objective is more easily met by observation-driven methods.

Other routinely used simulation methods exist that do not fall as neatly within the model-driven/observation-driven dichotomy. For example, in simulations produced by stochastic weather generators [Semenov and Barrow (1997), Wilks and Wilby (1999)], the observations are replaced with synthetic data drawn from a stochastic model meant to mimic the distribution of the observations. The stochastic weather generator can then be modified to account for changes predicted by a climate model. The drawback of this approach is that a statistical model for the observations is required in addition to a model for GCM projected changes, whereas observation-driven methods only require the latter. Synthetically generated observations will be less realistic than the observations themselves. Other related methods in the statistics literature also attempt to use statistical models to

blend information from observations with climate models to produce future simulations [e.g., Salazar et al. (2011)], but the proposed statistical models make very strong assumptions on the spatiotemporal distribution of the observations and the climate model realizations. Especially when projected changes from the historical climate are not very large, simulation methods should preserve features of the observed climate where possible. We therefore view observation-driven methods like the Delta method as likely to produce more realistic simulations than these methods as well.

We have advocated for observation-driven simulation methods, but an important limitation of the observation-driven Delta method described above is that it does not account for changes in variability (Figure 1, bottom row). Some extensions of the Delta method account for changes in marginal variance projected by a GCM [e.g., see again Hawkins et al. (2013)], but, again, since variability changes need not be uniform across all timescales of variation, changes in marginal variance are not a complete summary of GCM projected changes in variability. Leeds, Moyer and Stein (2015) introduced an extension of the Delta method that does account for changes in the full temporal covariance structure projected by a GCM, but their approach is applicable only for equilibrated climates, in which temperatures (after preprocessing for seasonality) can be assumed to be stationary in time. The Earth's climate, however, is and will continue to be in a transient state, in which temperatures will by definition be nonstationary in time. There is therefore an outstanding need for methods both to characterize changes in covariance in transient, nonstationary climates and to simulate temperatures in such climates.

In this work, we build on the work described in Leeds, Moyer and Stein (2015) to develop a methodology for generating observation-driven simulations of temperatures in future, transient climates that account for transient changes in both means and temporal covariances. In Figure 1, bottom row, our proposed method, unlike simple bias correction or the Delta method, both accounts for the relevant changes projected by the cartoon model and retains other distributional properties of the observations. Our method reduces to the Delta method in the case that the model predicts no changes in variability, and reduces to the method in Leeds, Moyer and Stein (2015) if the past and future climates are both in equilibrium. Since such a simulation uses projected changes in covariances from a GCM, our methodology must provide a way of modeling and estimating these changes in transient GCM runs. The transient, nonstationary setting adds substantial challenges, and so the statistical modeling of changes in covariance in transient GCM runs is a primary focus of this paper.

As a final complication, since GCMs are extremely computationally intensive, it is not possible to run a GCM under every scenario relevant for impacts assessments. In the absence of a run for a scenario of interest, impacts modelers may instead rely on a GCM emulator, a simpler procedure that produces, for example, mean temperatures that mimic what the GCM would have produced had it been

run. Our framework for simulations can use emulated rather than true GCM projections. For methods that emulate mean temperatures over forcing scenarios, see Castruccio et al. (2014) and references therein, and see the literature stemming from the pattern-scaling method of Santer et al. (1990). Much of the literature on climate model emulation has focused not on emulating model output across different forcing scenarios, but rather on emulating output with differing values of key climate model parameters (often for the purpose of selecting values of those parameters) [e.g., Bhat et al. (2012), Chang et al. (2014), Rougier et al. (2009), Sansó and Forest (2009), Sansó, Forest and Zantedeschi (2008), Williamson et al. (2013) and others]. While the statistical concerns related to emulating climate models in parameter space are somewhat different from those of emulating in scenario space, the general idea remains the same: that one may use available climate model runs to infer properties of a run that has not been produced. In our case, we require an emulator for the GCM changes in covariance in addition to a mean emulator. Our proposed statistical model can be used for this purpose, allowing our observation-driven procedure to simulate future temperatures in a potentially wide range of forcing scenarios.

Any simulation method that combines observations and model output (whether observation- or model-driven) involves the assumption that observations are less uncertain than is the output of GCMs. It is important to recognize that observational data products do themselves involve uncertainties that should be kept in mind when evaluating the appropriateness of a method for any particular use. In addition to intrinsic measurement uncertainty (e.g., calibration issues or time-varying changes), most datasets involve gridding data that are inhomogeneously distributed and come from different sources: raw observational data may be point-referenced (e.g., station data) or represent area averages (e.g., satellite measurements of radiances). Gridded data products are therefore affected by interpolation schemes and problems related to "spatial change of support" and misalignment [Gotway and Young (2002)], and care must be taken to appropriately combine raw observations to produce gridded products. To attempt to explicitly account for uncertainties, some observational data products are made available as ensembles [e.g., Morice et al. (2012)]. In many cases (including this work) the observational data products used are "reanalyses," in which information from different sources are combined with a climate/weather model to produce a self-consistent solution. Reanalyses are therefore also affected by the model and data assimilation schemes used. For further discussion of uncertainty in the observational record, see IPCC (2013), Chapter 2, especially Box 2.1, and references therein. In this paper we do not explicitly account for uncertainties associated with the observational record but assume that, in practice, the use of any method that combines models and observations also involves the appropriate evaluation of observational data products relative to raw model output. One method of evaluation is to repeat any procedure used with multiple data sources.

The remainder of this article is organized as follows. In Section 2 we motivate and describe our procedure for observation-driven simulations of future temperatures in transient climates that accounts for projected changes in both means and temporal covariances. In Section 3 we describe a GCM ensemble that we use to illustrate our methodology. In Section 4 we describe a statistical model for the changes in temporal covariances observed in this GCM ensemble that can be used as an emulator for these changes; we also discuss the estimation of this statistical model. In Section 5 we discuss results of applying our model to the GCM output and generating corresponding simulations, and evaluate the quality of our model in emulating the GCM projections. In Section 6 we give some concluding remarks and highlight areas for future research.

2. Observation-driven simulations of temperatures in future transient climates. Our goal is to provide a simulation of future temperatures in a transient climate under a known forcing scenario. In light of the preceding discussion, this simulation should reflect knowledge of the changes in the mean and covariance structure of future temperatures under that scenario, but should otherwise preserve properties of the observed temperature record.

Our proposed procedure is motivated by an idealization of the problem, supposing that the future changes in mean and temporal covariance structure are known. Following this motivation, we describe some modifications to the proposed procedure that we argue make the procedure more useful in practical settings when changes in mean and covariance must be estimated from, for example, GCM runs.

2.1. *Idealization.* Consider a family of multivariate (i.e., spatially referenced) Gaussian time series, $z_l^{(s)}(t)$ at times $t = \ldots, -1, 0, 1, \ldots$ and locations $l = 1, \ldots, L$, indexed by $s \in \mathcal{S}$, some set of scenarios. Write $\mu_l^{(s)}(t)$ for the unknown mean of $z_l^{(s)}(t)$ and assume that at each location, $z_l^{(s)}(t)$ has an unknown evolutionary spectrum, $a_l^{(s)}(t, \omega)$; for details on processes with evolutionary spectra, see Priestley (1981). Processes with temporally varying covariance structures in general have been discussed extensively in the literature. An overview of a theoretical framework for understanding locally stationary processes, closely tied to the Priestley model, can be found in Dahlhaus (2012) and the references therein. Our focus in this paper is on spectral methods because we view evolutionary spectra to be an intuitive way to characterize time-varying covariances and because the process's corresponding spectral representation has useful implications for our simulation procedure. Most importantly, $z_l^{(s)}(t)$ has, at each location and for each s, the spectral representation

$$z_l^{(s)}(t) = \mu_l^{(s)}(t) + \int_{-\pi}^{\pi} e^{i\omega t} \sqrt{a_l^{(s)}(t, \omega)}\, d\xi_l^{(s)}(\omega),$$

where $\xi_l^{(s)}(\omega)$ is a mean zero process with orthogonal increments and unit variance; that is, $E[d\xi_l^{(s)}(\omega)\, d\xi_l^{(s)}(\omega)^*] = d\omega$ and $E[d\xi_l^{(s)}(\omega)\, d\xi_l^{(s)}(\omega')^*] = 0$ for $\omega \neq \omega'$, with * denoting the complex conjugate. Here and throughout this paper, we restrict our attention to nonstationary processes with evolutionary spectral representations whose transfer functions, $\sqrt{a_l^{(s)}}$, are real and positive.

Suppose that we observe the time series under one scenario, $z_l^{(0)}(t)$, for times $t = 1, \ldots, N_0$. Call $z_l^{(0)}(t)$ the observed time series; given the observed time series, we would like to generate a simulation of the same length as the observations, but approximately equal in distribution to an unobserved time series, $z_l^{(s)}(t)$, for a given s. Since both $z_l^{(0)}(t)$ and $z_l^{(s)}(t)$ are Gaussian, there is a class of affine transformations of $z_l^{(0)}(t)$ that is equal in distribution to $z_l^{(s)}(t)$; indeed, writing $\Sigma_l^{(0)}$ and $\Sigma_l^{(s)}$ for the covariance matrices of the observed and unobserved time series at location l, we have that (marginally, at each location)

$$\mathbf{z}_l^{(s)} =_{\mathcal{D}} \boldsymbol{\mu}_l^{(s)} + (\Sigma_l^{(s)})^{1/2}(\Sigma_l^{(0)})^{-1/2}(\mathbf{z}_l^{(0)} - \boldsymbol{\mu}_l^{(0)})$$

for any matrix square root, where $\mathbf{x}$ denotes the vector with entries $x(t)$. While it is not immediately obvious that this fact is helpful, since the means and covariances of the two time series are unknown and at least for the unobserved time series cannot be directly estimated, we will describe a setting in which it is possible to compute this transformation (approximately) without fully knowing the means and covariances of the two time series.

The covariances of the observed and unobserved time series may be written as

$$(\Sigma_l^{(0)})_{t,t'} = \int_{-\pi}^{\pi} e^{i\omega(t-t')} \sqrt{a_l^{(0)}(t,\omega) a_l^{(0)}(t',\omega)^*}\, d\omega$$

and

$$(\Sigma_l^{(s)})_{t,t'} = \int_{-\pi}^{\pi} e^{i\omega(t-t')} \sqrt{a_l^{(s)}(t,\omega) a_l^{(s)}(t',\omega)^*}\, d\omega,$$

which follows immediately from the processes' spectral representations. Guinness and Stein (2013) showed that, under some regularity conditions on the evolutionary spectra, these matrices can be approximated as

$$\Sigma_l^{(0)} \approx C_{N_0}\left(\sqrt{a_l^{(0)}}\right) C_{N_0}\left(\sqrt{a_l^{(0)}}\right)^H$$

and

$$\Sigma_l^{(s)} \approx C_{N_0}\left(\sqrt{a_l^{(s)}}\right) C_{N_0}\left(\sqrt{a_l^{(s)}}\right)^H,$$

where H denotes the conjugate transpose and, generically for some function $A(t,\omega)$ in time and frequency, $C_N(A)$ is the $N \times N$ matrix with entries

$$C_N(A)_{t,j} = \sqrt{\frac{2\pi}{N}} A\big(t, 2\pi(j-1)/N\big) e^{2\pi i (j-1)t/N}$$

for $t, j = 1, \ldots, N$. [In the setting where A is constant in time, $C_N(A)$ is the inverse discrete time Fourier transform scaled by A and the result is the well-known result that the discrete time Fourier transform approximately diagonalizes the covariance matrix for a stationary time series observed at evenly spaced intervals.] The following transformation of $z_l^{(0)}(t)$ is therefore, marginally at each location, l, approximately equal in distribution to $z_l^{(s)}(t)$:

$$\mathbf{z}_l^{(s,0)} = \boldsymbol{\mu}_l^{(s)} + C_{N_0}\Big(\sqrt{a_l^{(s)}}\Big) C_{N_0}\Big(\sqrt{a_l^{(0)}}\Big)^{-1} (\mathbf{z}_l^{(0)} - \boldsymbol{\mu}_l^{(0)}). \tag{1}$$

The crucial observation, however, is that (1) can be computed exactly without fully knowing the means and covariances of the observed and unobserved time series. Indeed, suppose that what we are given are not the means and evolutionary spectra of the processes themselves, but some other substitute set of functions $\tilde{\mu}_l^{(s)}(t)$ and $\tilde{a}_l^{(s)}(t, \omega)$ satisfying, for each scenario s and at each location l,

$$\mu_l^{(s)}(t) - \tilde{\mu}_l^{(s)}(t) = c_l \quad \text{and} \quad \frac{a_l^{(s)}(t, \omega)}{\tilde{a}_l^{(s)}(t, \omega)} = k_l(\omega), \tag{2}$$

for some unknown constant c_l and some unknown function $k_l(\omega)$ that is constant in time. This situation is analogous to our actual predicament, where GCM runs are assumed to be more informative about changes than absolute levels; indeed, one consequence of the assumptions (2) is that the substitute means and evolutionary spectra change in the same way as their true counterparts, so, for instance, we may write

$$\Delta_l^{(s,0)}(t) \equiv \mu_l^{(s)}(t) - \mu_l^{(0)}(t) = \tilde{\mu}_l^{(s)}(t) - \tilde{\mu}_l^{(0)}(t)$$

and

$$\rho_l^{(s,0)}(t, \omega) \equiv \frac{a_l^{(s)}(t, \omega)}{a_l^{(0)}(t, \omega)} = \frac{\tilde{a}_l^{(s)}(t, \omega)}{\tilde{a}_l^{(0)}(t, \omega)},$$

for the known changes in means and covariance structures. The assumption that GCM mean temperatures are off by a constant compared to real temperatures is essentially the assumption underlying both simple bias correction and the Delta method as described in Section 1, and we view the assumption on the evolutionary spectra as a natural extension to covariances; all existing simulation methods that we are aware of implicitly or explicitly make the same or similar assumptions (except the simple Delta method, which assumes no changes in variability at all).

Under these assumptions, (1) may be rewritten as

$$\mathbf{z}_l^{(s,0)} = \boldsymbol{\mu}_l^{(0)} + \boldsymbol{\Delta}_l^{(s,0)} + C_{N_0}\Big(\sqrt{\tilde{a}_l^{(s)}}\Big) C_{N_0}\Big(\sqrt{\tilde{a}_l^{(0)}}\Big)^{-1} (\mathbf{z}_l^{(0)} - \boldsymbol{\mu}_l^{(0)}), \tag{3}$$

where, to reiterate, (1) and (3) are equal under the assumptions (2) because $C_{N_0}(\sqrt{\tilde{a}_l^{(s)}}) = C_{N_0}(\sqrt{a_l^{(s)}})\mathrm{diag}(1/k_l)$, where $\mathrm{diag}(1/k_l)$ is the diagonal matrix

with entries $1/k_l(\omega_j)$, so

$$C_{N_0}\left(\sqrt{\tilde{a}_l^{(s)}}\right)C_{N_0}\left(\sqrt{\tilde{a}_l^{(0)}}\right)^{-1} = C_{N_0}\left(\sqrt{a_l^{(s)}}\right)C_{N_0}\left(\sqrt{a_l^{(0)}}\right)^{-1}.$$

In light of (3), our proposed simulation can be computed as long as one knows (or, more realistically, can estimate) just the mean of the observed time series as well as the substitute evolutionary spectra and changes in mean. The procedure described by (3) is what is illustrated in the bottom right panel of Figure 1.

In the case that there are no changes in covariance structure, so $a_l^{(s)}(t,\omega) = a_l^{(0)}(t,\omega)$ and the same for their substitute counterparts, the simulation procedure (3) is equivalent to the Delta method as described in Section 1. In the case that both $a_l^{(s)}(t,\omega)$ and $a_l^{(0)}(t,\omega)$ are constant in time, so the de-meaned time series are stationary, the procedure is the same as that described in Leeds, Moyer and Stein (2015). Our proposal is therefore a generalization of those two procedures, describing an observation-driven simulation that transforms one observed time series (possibly itself from a transient climate) to a simulation under a new (future, transient) scenario.

2.2. *Practical modifications to idealized procedure.* In practice, we do not actually know even substitute versions of the future changes in mean and covariance structure, so the procedure we have described in the preceding section must be modified to be made useful.

A key assumption underlying our methodology is that GCM runs are informative about at least some aspect of the changes in mean and covariance structure of the real temperatures; however, it need not be true that the assumptions (2) will be satisfied by taking $\mu_l^{(s)}(t)$ and $a_l^{(s)}(t,\omega)$ to be the means and evolutionary spectra corresponding to real temperatures and taking $\tilde{\mu}_l^{(s)}(t)$ and $\tilde{a}_l^{(s)}(t,\omega)$ to be those corresponding to temperatures under GCM runs. One possible objection to these assumptions is that both the observations and the GCM runs will exhibit nonstationarity in mean and variance due to seasonality, and it is at least plausible that the GCM representation of these seasonal cycles will differ from that of the observations. Leeds, Moyer and Stein (2015) argued that the seasonality can be reasonably represented as a uniformly modulated process [see Priestley (1981)] plus a mean seasonal cycle. That is, writing $T_l^{(s)}(t)$ for the true temperatures at time t and location l in scenario s, and d for the day of the year, we assume that

$$T_l^{(s)}(t) = \mu_l^{(s)}(t) + m_l^{(T)}(d) + D_l^{(T)}(d)\big(z_l^{(s)}(t) - \mu_l^{(s)}(t)\big),$$

where $m_l^{(T)}(d)$ and $D_l^{(T)}(d)$ represent seasonal cycles in means and marginal variances, and $z_l^{(s)}(t)$ has mean $\mu_l^{(s)}(t)$ and evolutionary spectrum $a^{(s)}(t,\omega)$ as above; assume a similar form for the GCM runs. [In the following, we will allow $\mu_l^{(s)}(t)$ to reflect changes in the mean seasonal cycle from $m_l^{(T)}(d)$, but for simplicity will assume that $a^{(s)}(t,\omega)$ has no seasonal structure; see Section 3.1 for details.]

We estimate the seasonal cycles in mean and variability in the observations according to the methods described in Leeds, Moyer and Stein (2015); the mean seasonal cycle is modeled with the first ten annual harmonics and estimated via least squares, whereas the annual cycle in variability is estimated by a normalized moving average of windowed variances that has been averaged across years. We will assume that (2) is reasonable, taking $\mu_l^{(s)}(t)$, $a^{(s)}(t,\omega)$, $\tilde{\mu}_l^{(s)}(t)$ and $\tilde{a}^{(s)}(t,\omega)$ to be the means and evolutionary spectra of the deseasonalized components of real and GCM temperatures.

Even assuming that (2) holds for the deseasonalized components of observed and GCM temperatures, what we are given are the real and GCM temperatures themselves, not their means and evolutionary spectra. As such, the quantities necessary to compute (3) must be estimated using the available data. While it would be possible to estimate the corresponding evolutionary spectra from the GCM runs directly, note that (3) works for any substitute function in time and frequency that, for each frequency, is proportional to the true evolutionary spectra at all times. If such a function must be estimated, there is presumably a statistical advantage to estimating a function that is relatively flat across frequencies. In GCM experiments, it is fairly typical to have a control run under an equilibrated (often preindustrial) climate, in which at least the deseasonalized temperatures can be viewed as a stationary process. Writing $s = B$ for this equilibrated scenario, and $\tilde{a}_l^{(B)}(\omega) \equiv \tilde{a}_l^{(B)}(t,\omega)$ for the corresponding spectral density of the deseasonalized component of the equilibrated GCM temperatures, then if (2) holds, it will also be true that we can write

$$\rho_l^{(s,B)}(t,\omega) \equiv \frac{a^{(s)}(t,\omega)}{a^{(B)}(\omega)} = \frac{\tilde{a}^{(s)}(t,\omega)}{\tilde{a}^{(B)}(\omega)},$$

in which case $a^{(s)}(t,\omega)/\rho_l^{(s,B)}(t,\omega) = a^{(B)}(\omega)$ and (2) still holds if one replaces $\tilde{a}^{(s)}(t,\omega)$ with $\rho_l^{(s,B)}(t,\omega)$. Moreover, we expect that the functions $\rho_l^{(s,B)}(t,\omega)$ will be much flatter than the functions $\tilde{a}_l^{(s)}(t,\omega)$ over the range of scenarios considered reasonable, so we expect that there should be some advantage in estimating these ratios rather than the evolutionary spectra themselves from the GCM runs.

Writing $T_l^{(s,0)}(t)$ for our simulation of the true temperatures under scenario s, our proposed procedure is therefore

$$\begin{aligned}\mathbf{T}_l^{(s,0)} &= \hat{\boldsymbol{\mu}}_l^{(0)} + \hat{\mathbf{m}}_l^{(T)} + \hat{\boldsymbol{\Delta}}_l^{(s,0)} \\ &\quad + \operatorname{diag}(\hat{\mathbf{D}}_l^{(T)}) C_{N_0}\big(\sqrt{\hat{\rho}^{(s,B)}}\big) C_{N_0}^{-1}\big(\sqrt{\hat{\rho}^{(0,B)}}\big)(\hat{\mathbf{z}}_l^{(0)} - \hat{\boldsymbol{\mu}}_l^{(0)}),\end{aligned} \tag{4}$$

where $\hat{x}$ generically represents an estimate of the quantity x. In words, the procedure is, in order, (i) estimate and remove seasonality and mean trend in the observational record; (ii) estimate the future changes in mean and marginal spectra using an ensemble of GCM runs; (iii) decorrelate the detrended and deseasonalized

observations using the estimated substitute function, $\hat{\rho}^{(0,B)}$, obtained in step (ii); (iv) apply the estimated changes in spectra, $\hat{\rho}^{(s,B)}$, to the decorrelated data and invert the transformation in (iii); and (v) replace the seasonal cycles in means and variability, and add the new changes in mean.

The practicality of (4) depends both on our ability to obtain good estimates of all of the involved quantities and on our ability to compute the simulation efficiently. Castruccio et al. (2014) and Leeds, Moyer and Stein (2015) collectively describe methods that essentially can be used to estimate all of the necessary quantities in the procedure except, crucially, the changes in evolutionary spectra. In the following, we will discuss modeling and estimating these functions from an ensemble of GCM runs. The particular statistical model we develop allows for efficient computation of the simulation.

3. Description of GCM ensemble. We study changes in the distribution of daily temperatures in an ensemble of GCM runs made with the Community Climate System Model Version 3 (CCSM3) [Collins et al. (2006), Yeager et al. (2006)] at T31 atmospheric resolution (a 48×96 grid with a resolution of approximately $3.75° \times 3.75°$) and a 3° resolution for oceans. All runs require a long spin up; the realizations in our ensemble are initialized successively at ten-year intervals of the NCAR b30.048 preindustrial control run. Each transient realization is then forced by historical CO_2 concentrations (herein, $[CO_2]$) from years 1870–2010, at which point the ensemble branches into three future increasing $[CO_2]$ scenarios for the years 2010–2100, which we name the "high," "medium" and "low" concentration scenarios (Figure 2). For each scenario, we have a modest number

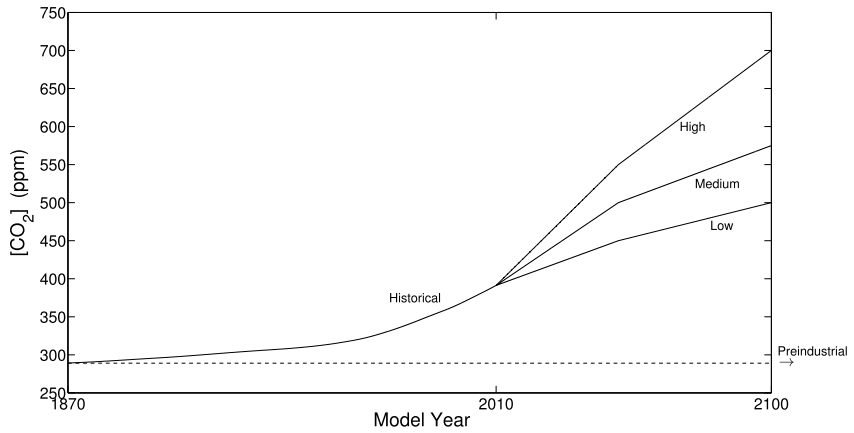

FIG. 2. *GCM ensemble* $[CO_2]$ *trajectories. The historical scenario begins in* 1870 *and follows observed* $[CO_2]$ *until* 2010, *after which it branches into the three future scenarios increasing at different rates until* 2100. *The preindustrial run maintains* 1870*-level* $[CO_2]$ *until the year* 4600, *but we use only the last* 1500 *years of that run. The ensemble includes eight realizations each under the historical, high and low scenarios, five under the medium scenario, and one under preindustrial* $[CO_2]$.

of realizations (eight realizations from the historical, high and low scenarios, and five realizations from the medium scenario), so the transient ensemble consists of about 1.1 million observations at each grid cell, or about 5 billion observations in total. As is typical, we will assume throughout that the ensemble members can be viewed as statistically independent realizations due to the system's sensitivity to initial conditions.

The focus of our investigation is on changes in temporal covariance structure in transient (nonstationary) runs of the GCM, but for the reasons described in Section 2.2, it is helpful to have a representation of the model's climate in a baseline, equilibrated state. For this purpose, we use a single, long run forced under preindustrial $[CO_2]$ (289 ppm) for an additional 2800 years past the control run initialization to ensure that the run is fully equilibrated, from which we use the last 1500 years, or about 0.5 million days, for a total of about 2.5 billion observations under preindustrial $[CO_2]$.

In the following, we will index the members of the GCM ensemble by their $[CO_2]$ scenario, $s \in \{B, 0, H, M, L\}$, denoting, respectively, the baseline preindustrial, historical, high, medium and low scenarios.

3.1. *Data preprocessing.* The primary inferential aim of this work is to obtain estimates of $\rho_l^{(s,B)}(t, \omega)$, the changes in marginal evolutionary spectra of the deseasonalized component of daily temperatures in the GCM under scenario s compared to the preindustrial climate. The GCM runs have, accordingly, been preprocessed to remove means and seasonal cycles of variability.

As with the observed temperatures in Section 2, we represent temperatures in the preindustrial run at each grid cell as a uniformly modulated process plus a mean seasonal cycle and retain the stationary component of this process. That is, write $y_l^{(B)}(t)$ for the temperature in the raw, equilibrated preindustrial GCM run at time t and location l, and again write d for the day of the year (the GCM does not have leap years, so $d \in \{1, \ldots, 365\}$). We represent these as

$$y_l^{(B)}(t) = \tilde{m}_l(d) + \tilde{D}_l(d) x_l^{(B)}(t),$$

where $\tilde{m}_l(d)$ and $\tilde{D}_l(d)$ are the estimated seasonal cycles in mean and marginal variance, and $x_l^{(B)}(t)$ is assumed to be stationary in time. The mean seasonal cycle and the seasonal cycle of marginal variance are estimated as described in Leeds, Moyer and Stein (2015), as also in the preceding section for the observational data. We retain $x_l^{(B)}(t)$, the deseasonalized component.

Temperatures in the transient runs, on the other hand, will in general have an evolving mean in addition to nonstationarity due to seasonality. Write $y_{l,r}^{(s)}(t)$ for the temperature in the rth realization of the transient scenario s at time t and location l, and assume the representation

$$y_{l,r}^{(s)}(t) = \tilde{m}_l(d) + \tilde{\mu}_l^{(s)}(t) + \tilde{D}_l(d) x_{l,r}^{(s)}(t),$$

where $\tilde{\mu}_l^{(s)}(t)$ represents an estimate of the evolving mean under scenario s (possibly including changes in the mean seasonal cycle) and $x_{l,r}^{(s)}(t)$ is assumed to be some mean zero, but nonstationary, process. For simplicity we assume that the seasonal cycles of marginal variability do not evolve in time [overall marginal variability is still allowed to change in $x_{l,r}^{(s)}(t)$, but such changes are assumed the same for each season. While the change in mean is needed for the simulation (4) (see Supplement S1 for details on its estimation [supplementary material Poppick et al. (2016)]), we would like to work with mean zero processes to estimate the changes in covariance structure. We therefore first remove from each transient realization the scenario average:

$$\check{y}_{l,r}^{(s)}(t) = y_{l,r}^{(s)}(t) - \frac{1}{R_s}\sum_{k=1}^{R_s} y_{l,k}^{(s)}(t),$$

where R_s is the number of realizations in the ensemble under scenario s. The resulting contrasts, $\check{y}_{l,r}^{(s)}(d)$, have mean zero, but still exhibit seasonal cycles in marginal variance. We thus retain the deseasonalized contrasts

$$q_{l,r}^{(s)}(t) = \frac{\check{y}_{l,r}^{(s)}(t)}{\tilde{D}_l(d)}. \tag{5}$$

While we view each run, $y_{l,r}^{(s)}(t)$, as independent, the contrasts, $q_{l,r}^{(s)}(t)$, are of course not independent across realizations within a given scenario.

We assume that the deseasonalized component of the preindustrial run, $x_l^{(B)}(t)$, has unknown marginal spectral density $\tilde{a}_l^{(B)}(\omega)$, and the deseasonalized component of the transient runs, $x_{l,r}^{(s)}(t)$, has unknown evolutionary spectrum $\tilde{a}_l^{(s)}(t,\omega)$. While $x_l^{(B)}(t)$ and $x_{l,r}^{(s)}(t)$ will not be equal in distribution to the (deseasonalized) real-world temperatures, past or future, we assume that the true changes in evolutionary spectra under scenario s are equal to those of the GCM, so the deseasonalized GCM and observed temperatures satisfy (2) and, in particular,

$$\rho_l^{(s,B)}(t,\omega) \equiv \frac{a_l^{(s)}(t,\omega)}{a_l^{(B)}(\omega)} = \frac{\tilde{a}_l^{(s)}(t,\omega)}{\tilde{a}_l^{(B)}(\omega)}.$$

In the following section we discuss modeling and estimating these changes in evolutionary spectra.

4. GCM projected changes in temporal covariance. We describe a methodology for modeling and estimating the changes in covariance structure in a GCM as a function of a $[CO_2]$ scenario. Our goal is not only to describe the changes in covariance in scenarios within our ensemble, but also to provide an emulator for the GCM changes in covariance for scenarios for which we have no runs. To the extent that the model we propose describes the GCM changes across the range of

$[CO_2]$ scenarios in our ensemble, the resulting emulator may be expected to provide good predictions of the GCM changes, at least for scenarios in some sense within the range spanned by our ensemble.

4.1. *A model for GCM changes in temporal covariance.* An important insight stated in Castruccio et al. (2014) is that changes in the distribution of temperatures in transient GCM runs under a $[CO_2]$ forcing scenario should be describable in terms of the past trajectory of $[CO_2]$. More specifically, writing $[CO_2](t)$ for the CO_2 concentration at time t, the distribution of temperature at time t is determined by the function

$$f(t') = [CO_2](t - t'), \qquad \text{for } t' > 0,$$

where f does not depend on t, so one does not need a different emulator for every time t. Providing useful statistical emulators for changes in the distribution of temperatures in transient GCM runs then depends on our ability to find useful functionals of the past $[CO_2]$ trajectory that help explain those changes.

One potentially useful summary of the past trajectory of $[CO_2]$ for a given scenario is in fact the change in regional mean temperature relative to the preindustrial climate. We denote this change as $\bar{\Delta}_S^{(s,B)}(t)$ for region S. In this work, we have subdivided the T31 grid into the same 47 regions as in Castruccio et al. (2014), chosen to be relatively homogeneous but still large enough to substantially reduce inter-annual variations. We estimate $\bar{\Delta}_S^{(s,B)}(t)$ in each region using a modification of the mean emulator described there (see Supplement S1 [Poppick et al. (2016)]).

While the changes in regional mean temperature are themselves useful summaries of the past trajectory of $[CO_2]$, it need not be true that temporal covariance structures will be the same if $\bar{\Delta}_S^{(s,B)}(t) = \bar{\Delta}_S^{(s',B)}(t')$ for two scenarios s and s' at two different time points t and t'. In particular, the rate of change of the evolution of regional mean temperatures $[\partial t \bar{\Delta}_S^{(s,B)}(t)$ for scenario $s]$ may capture some additional aspect of the changing climate that is also relevant for explaining changes in covariances.

We have indeed found that the following model usefully describes the changes in temporal covariances in scenarios in our ensemble:

$$\log \rho_l^{(s,B)}(t, \omega) = \delta_{l0}(\omega)\bar{\Delta}_S^{(s,B)}(t) + \delta_{l1}(\omega)\partial_t \bar{\Delta}_S^{(s,B)}(t). \tag{6}$$

In the case that $\delta_{l0}(\omega)$ and $\delta_{l1}(\omega)$ are constant functions, for example, (6) describes a uniformly modulated process. More generally, $\delta_{l0}(\omega)$ and $\delta_{l1}(\omega)$ describe the patterns of changes in variability across frequencies associated with changes in regional mean temperature and the rate of change of regional mean temperature, respectively.

Since each $\delta_{li}(\omega)$ is not scenario-dependent, model (6) can be thought of as an emulator for the GCM changes in covariance structure. That is, given an emulator for the regional mean temperature changes in the scenario of interest, (6) provides

a prediction of the GCM changes in covariance structure under that scenario. In Section 5 we will discuss how well this model describes changes across the scenarios in our ensemble. Note that a model like (6) is unlikely to hold generically for all $[CO_2]$ scenarios. In particular, such a model would be unlikely to fully capture the changes in variability in scenarios where $[CO_2]$ changes instantaneously; such scenarios are typically not considered realistic. Additionally, since the changes in covariance in (6) depend on the $[CO_2]$ trajectory through the corresponding *changes* in mean, this model will not fully capture changes in variability that depend on *absolute* temperatures through, for example, phase changes between ice and water (see Figure 5 and discussion in Section 5.2). The model will also not fully capture GCM behavior if that behavior involved abrupt changes in the distribution of temperatures even under relatively smooth forcing scenarios (nonlinear responses to forcing); however, the GCM we study does not exhibit such behavior over the range of $[CO_2]$ scenarios we study. We have found that the model is a useful description of changes in variability in scenarios like those in the ensemble we use here, where $[CO_2]$ changes slowly and relatively smoothly over time and in locations not involving changing ice margins over the course of the scenario.

4.1.1. *Estimating* $\delta_{li}(\omega)$. To estimate the functions $\delta_{l0}(\omega)$ and $\delta_{l1}(\omega)$, we adopt the intuitive approach for likelihoods for processes with evolutionary spectra where the usual periodogram in the Whittle likelihood is replaced with local periodograms over smaller blocks of time [Dahlhaus (1997)]. While we view the local Whittle likelihood approach as most suitable in our setting, several other alternative methods for estimating evolutionary spectra have been proposed. Neumann and von Sachs (1997) used a wavelet basis expansion; Ombao et al. (2002) used smooth, localized complex exponential basis functions; Dahlhaus (2000) proposed another likelihood approximation that replaces the local periodogram in the earlier work with the so-called pre-periodogram introduced by Neumann and von Sachs (1997); Guinness and Stein (2013) provided an alternative generalization of the Whittle likelihood that they argued, at least in the settings they studied, is more accurate than the approximations given by either Dahlhaus (1997) or Dahlhaus (2000). However, an advantage of the local Whittle likelihood approach is that, in addition to being intuitive, the corresponding score equations are computationally easier to solve in our setting when the evolutionary spectra evolve very slowly in time so the local periodograms can be taken over large blocks of time. Computation is an especially important consideration when estimating a semiparametric model such as (6). Furthermore, the results from Guinness and Stein (2013) suggest that the local Whittle likelihood approach may yield point estimates that are close to optimal even when the likelihood approximation itself is inaccurate, whereas, for example, they demonstrated that the approach based on the pre-periodogram can give unstable estimates.

In this work, we interpret the local Whittle likelihood approach as follows. We divide each contrast time series, $q_{l,r}^{(s)}(t)$, defined in (5) and of length N_s, into blocks

of length M (for simplicity take M to be a common factor of each N_s). In our setting, we take $M = 10$ years, but since temperature variability changes very slowly over time in the scenarios we analyze, the conclusions are not very sensitive to the choice of M; the results are essentially the same taking $M = 5$ years or $M = 30$ years, for example. Upon choosing M, then for the time block, location, realization and scenario indexed by b, l, r and s, respectively, define the local periodogram of the contrast time series at frequencies $\omega_j = 0, 2\pi/M, \ldots, 2\pi$ as

$$I^{(s)}_{b,l,r}(\omega_j) = \frac{1}{2\pi M}\left|\sum_{t=1}^{M} q^{(s)}_{l,r}\big(t + M(b-1)\big)e^{-it\omega_j}\right|^2. \tag{7}$$

It is straightforward to show that the Whittle likelihood for each time block, location and scenario depends on each $I^{(s)}_{b,l,r}(\omega_j)$ only through the average across realizations,

$$\bar{I}^{(s)}_{b,l}(\omega_j) = \frac{1}{R_s}\sum_{r=1}^{R_s} I^{(s)}_{b,l,r}(\omega_j). \tag{8}$$

Likewise, for the deseasonalized preindustrial run, define its periodogram as

$$I^{(B)}_{l}(\omega_j) = \frac{1}{2\pi N_B}\left|\sum_{t=1}^{N_B} x^{(B)}_{l}(t)e^{-it\omega_j}\right|^2. \tag{9}$$

In our setting, since $M < N_B$, $I^{(s)}_{b,l,r}(\omega_j)$ is defined on a coarser frequency scale than is $I^{(B)}_{l}(\omega_j)$, so for the purposes of estimating changes in spectra, it may be natural to aggregate the baseline periodogram to the coarser scale, that is, write

$$\bar{I}^{(B)}_{l}(\omega_j) = \frac{M}{N_B}\sum_{k:-N_B/2M\le k<N_B/2M} I^{(B)}_{l}\left(\frac{2\pi(j+k)}{N_B}\right). \tag{10}$$

An approximate likelihood under model (6), marginally at each location l, may then be written as the sum of the local Whittle likelihoods of the transient runs and the Whittle likelihood corresponding to the aggregated periodogram of the baseline run (under the usual approximation that the periodogram ordinates are independent at distinct Fourier frequencies):

$$\begin{aligned}\mathcal{L}_l(\theta) = -\frac{1}{2}\sum_{s,b,j}\Big\{&(R_s-1)\big(\log\tilde{a}^{(B)}_{l}(\omega_j) + \bar{\Delta}^{(s,B)}_{b}\delta_{l0}(\omega_j) + \partial_t\bar{\Delta}^{(s,B)}_{b}\delta_{l1}(\omega_j)\big)\\ &+ R_s\bar{I}^{(s)}_{b,l}(\omega_j)e^{-(\log\tilde{a}^{(B)}_{l}(\omega_j)+\bar{\Delta}^{(s,B)}_{b}\delta_{l0}(\omega_j)+\partial_t\bar{\Delta}^{(s,B)}_{b}\delta_{l1}(\omega_j))}\Big\}\\ &- \frac{M}{2}\sum_{j}\big\{\log\tilde{a}^{(B)}_{l}(\omega_j) + \bar{I}^{(B)}_{l}(\omega_j)/\tilde{a}^{(B)}_{l}(\omega_j)\big\},\end{aligned} \tag{11}$$

where $\theta = (\tilde{a}^{(B)}, \delta_{l0}, \delta_{l1})$ and where $\bar{\Delta}_b^{(s,B)}$ and $\partial_t \bar{\Delta}_b^{(s,B)}$ correspond to the values of $\bar{\Delta}^{(s,B)}(t)$ and $\partial_t \bar{\Delta}^{(s,B)}(t)$ for t at the midpoint of time block b. Here the $(R_s - 1)$ factor multiplying the log-determinant approximation takes into account that the contrasts, $q_{l,r}^{(s)}(t)$, are obtained by subtracting off the scenario average across realizations; see Castruccio and Stein (2013) for details.

The estimator maximizing (11), say,

$$\theta_l^* = \arg\max_{\theta} \mathcal{L}_l(\theta), \tag{12}$$

will yield very rough estimates of the functions $\tilde{a}_l^{(B)}(\omega)$, $\delta_{l0}(\omega)$ and $\delta_{l1}(\omega)$ because no smoothness has been enforced across frequencies. The baseline spectrum, $\tilde{a}_l^{(B)}(\omega)$, is not of particular interest to us, as this function is not required for the simulation (4). On the other hand, maximizing (11) is clearly inadequate for estimating the functions of interest, $\delta_{l0}(\omega)$ and $\delta_{l1}(\omega)$.

A common approach for nonparametrically estimating the spectral density of a stationary process is to smooth its periodogram either by kernel methods or by penalized likelihood methods. For estimating ratios of spectra between two stationary processes, Leeds, Moyer and Stein (2015) adopted a penalized likelihood approach whereby the penalty enforced smoothness in the ratio. Here, we opt to smooth the rough estimates, δ_{l0}^* and δ_{l1}^*, using kernel methods; that is, for $i = 0, 1$ write as the final estimate for δ_{li}

$$\hat{\delta}_{li}(\omega_j) = \sum_k w_{k,j,i} \delta_{li}^*(\omega_{j+k}), \tag{13}$$

where $w_{k,j,i}$ are weights (possibly varying with j and i) satisfying $\sum_k w_{k,j,i} = 1$ for each i and j. In practice, we use weights corresponding to a kernel with a variable bandwidth that is allowed to decrease at lower frequencies. The reason for the variable bandwidth is that in the GCM runs we have analyzed, we have observed that the log ratio of spectra is typically less smooth at very low frequencies compared to higher frequencies. For details on the form of the weights and the bandwidth selection procedure we use to choose them, see Supplement S2 [Poppick et al. (2016)]. While the penalized likelihood approach described in Leeds, Moyer and Stein (2015) may be adapted for this setting, we view the kernel smoothing approach as more straightforward, especially when allowing for variable bandwidths, and have found that the approaches yield similar estimates when the bandwidth of the kernel is constant.

Approximate pointwise standard errors for each $\hat{\delta}_{li}(\omega_j)$, and for the corresponding estimate of $\log \rho_l^{(s,B)}(t, \omega_j)$, may also be computed; these are described in Supplement S3 [Poppick et al. (2016)]. Having estimated our model, we need to compute the observation-driven simulations. Computing (4) efficiently is important; this is described in Supplement S4.

5. Results. In this section we show results from applying the procedures described in the previous sections. We first estimate the model described in Section 4 using our ensemble of CCSM3 runs described in Section 3. We then investigate the success of our proposed model in describing the changes in covariances in our GCM ensemble, evaluate the quality of our model when used as an emulator, and describe insights into the climate system that our estimated model provides. As an illustration, we use an observational data product to build a simulation of future temperatures via the methods outlined in Section 2.

In the simulation, we use temperatures from the NCEP-DOE Climate Forecast System Reanalysis (CFSR) [Saha et al. (2010)] as a surrogate for observational data. CFSR is the latest version of the global reanalysis produced by the National Centers for Environmental Prediction (NCEP). The reanalysis is run at T62 resolution (about a 1.875° grid); we regrid to T31 to match the resolution of our model output using an area-conserving remapping scheme. Validation studies suggest that modern reanalyses, including CFSR, have relatively small mean biases and variability discrepancies relative to station observations [Decker et al. (2012)], and CFSR appears, for example, to better represent inter-annual variability than older NCEP reanalyses [Wang et al. (2011)]. Nevertheless, as noted in Section 1, since there are differences between observational products and since our method does not account for uncertainties in the observations themselves, it is advisable for users to explore the effect that the choice of data product has on the resulting simulation.

5.1. *Model changes in variability.* In CCSM3, changes in variability in evolving climates can be primarily characterized using changes in mean temperature, with a smaller contribution by the rate of change of warming [corresponding to terms δ_{l0} and δ_{l1} in (6), respectively]. As a consequence, the projected patterns of changes in variability at a given time in a given future scenario largely correspond to the patterns observed in Leeds, Moyer and Stein (2015): the GCM projects decreases in short timescale variability at most locations, but increases in longer timescale variability in some regions, especially at lower latitudes (Figure 3, left).

The differences in variability between scenarios due to different rates of warming are small compared to the overall projected changes in variability, but also exhibit patterns. To illustrate, we compare changes in variability under the low scenario at year 2100 to the corresponding changes under the high scenario in the year of that scenario experiencing the same regional mean temperatures as at 2100 in the low scenario (Figure 3, right); this year varies by region, ranging from 2037 to 2044. An analogous figure is given in Supplement S5 [Poppick et al. (2016)] that shows the estimated changes in variability in each of the three scenarios at years corresponding to the same change in regional mean temperature. In about 75% of all locations, and especially in mid- and high-latitude ocean locations, the changes in variability under the high scenario are larger than under the low scenario. Larger changes under the high scenario than under the low scenario are an indication that

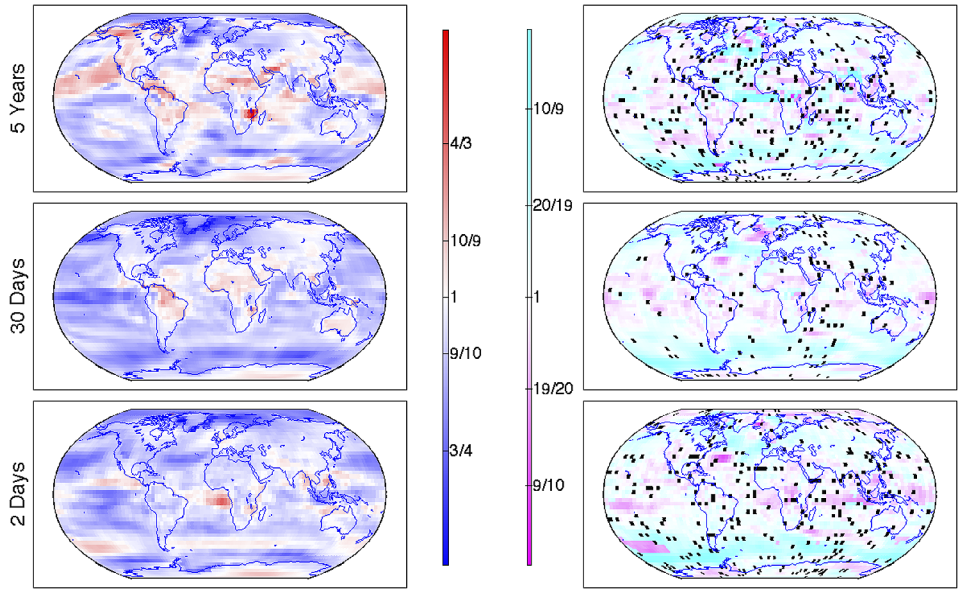

FIG. 3. *Left, estimates of changes in marginal spectra, at three frequencies, for the low scenario at model year* 2100 *compared to the preindustrial climate* [*i.e.*, $\rho_l^{(L,B)}(t,\omega)$ *at year* 2100 *and the specified periods*]. *Red indicates an increase in variability and blue a decrease in variability. Right, estimates of* $(\rho_l^{(H,B)}(t',\omega)/\rho_l^{(L,B)}(t,\omega))^{\text{sign}_{l,t,\omega}}$ *for* t' *corresponding to the model time under the high scenario with the same change in regional mean temperature as at year* 2100 *in the low scenario, where* $\text{sign}_{l,t,\omega}$ *is the sign of the log ratio at that location, time and frequency. Magenta grid cells indicate smaller changes in variability under the high scenario at the same temperature, whereas the cyan grid cells indicate bigger changes in variability.* (*Black grid cells indicate the roughly* 5% *of locations where the two estimates differ in sign, so comparing the relative magnitude of changes is not meaningful*). *Figure* S3 *repeats the left column maps for all the low, medium and high scenarios.*

variability changes are projected to be larger in a transient warming climate than in an equilibrated climate at the same temperature.

To illustrate how these changes in covariance structure are used in our proposed simulation, we simulate temperatures under the high scenario at a single grid cell in the Midwestern United States (Figure 4, which shows the observations in 2009–2010, our simulation 89 years in the future, and output from one of the GCM runs in the same timeframes). Mean temperatures warm, more strongly in the winter than in the summer at this location, and temporal variability decreases overall. More specifically, variability is projected to modestly decrease at higher frequencies and slightly increase at lower frequencies. At low frequencies, the projected log ratios are within two standard errors of zero, but at high frequencies are significantly smaller than zero. The extent to which such changes are important will of course depend on the impact domain of interest, and we have not carried out studies on specific events of potential interest (for example, hot spells).

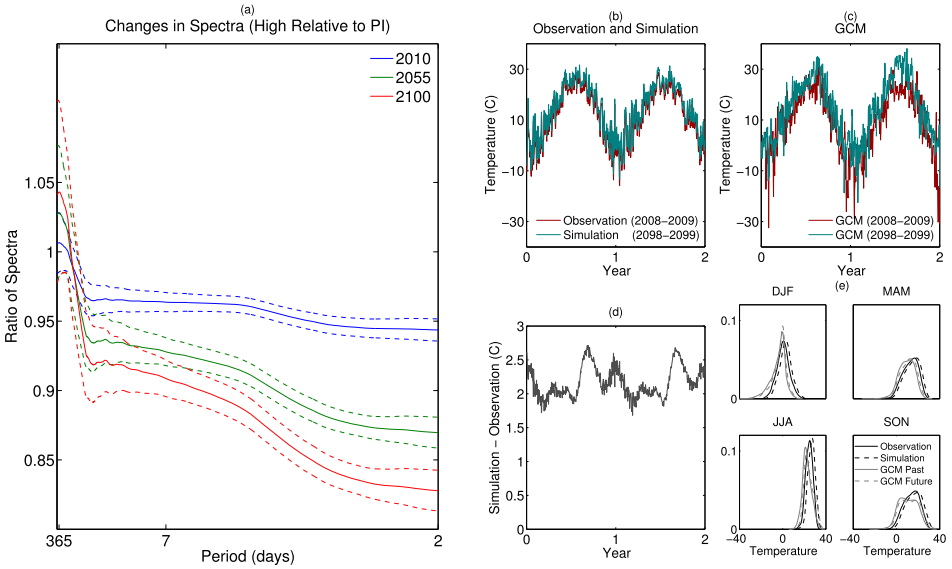

FIG. 4. (a) *Estimates of* $\rho_l^{(H,B)}(t,\omega)$ *for years* 2010, 2055 *and* 2100, *at a Midwestern United States grid cell* (*dashed curves at* $\pm$ *two standard errors on the log scale*). (b) *Part of the corresponding simulation computed by transforming the observational data at this grid cell via* (4); *the simulation was computed for the whole length of the observational data, but only the last two years are displayed*. (c) *A run of the GCM in the years corresponding to the simulation*. (d) *The difference between the observations and the simulation in panel* (b). *The overall shift upward in the simulation is due to increasing mean temperature. Most of the long timescale fluctuations in the bottom panel are due to changes in the seasonal cycle: at this location, temperatures are projected to warm more in winter months than in summer months. The short timescale fluctuations on the order of* 0.1 *degrees in the difference are due to changes in variability, which decreases in the future simulation*. (e) *Marginal densities by season* (*labeled by corresponding months*) *for the observations in* 2008–2009, *the simulation from* 2098–2099, *the GCM from the same years under the historical forcing and the high future scenario*.

The distribution of temperatures in the GCM differs strongly from that in the observations, with differences evident by eye in the raw time series and corresponding marginal densities. For example, the GCM has a stronger seasonal cycle than the observations and simulation, and greater variability in the winter months. See Supplement S5 [Poppick et al. (2016)] for additional comparisons of the space-time covariance structures of the observations and the GCM runs: typically, we have found that temperatures in nearby grid cells are more coherent in the GCM than in the observations, and that the coherences do not change much between the historical period and the end of the high scenario (Figures S4–S7). Our simulation procedure does not change the coherence structure of the observations. An animation of the full, global simulation is also given in the supplementary materials, demonstrating that our procedure yields realistic-looking simulations. Collectively, this forms an argument for our procedure, which preserves features of the observations.

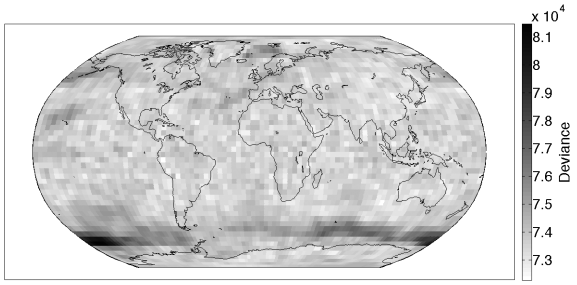

FIG. 5. *Deviances, comparing the approximate likelihood under our estimated model to that under the saturated model where the spectrum in each time block, scenario and frequency has its own parameter. The number of observations at each location is about* 1.6 *million days. The regions showing the largest deviances are those where changes in sea ice have a strong influence on variability; in such locations, our model based on changes in mean temperature cannot be expected to be a fully adequate description of changes in variability.*

5.2. *Assessing model fit and quality of emulation.* To assess different aspects of how well our model describes the changes in covariance structure in CCSM3 in evolving climates, we show three diagnostics. First, we address in which geographic locations the model performs relatively better or worse. Second, we ask how well the statistical model performs as an emulator for a scenario on which the model has not been trained. Finally, we show the extent to which the rate of change of mean warming improves the quality of emulation over the simpler model where changes in covariance are explained solely by changes in mean temperature.

To examine in which locations the model performs best and worst, we compare the deviances of our model at each location (Figure 5); recall that the deviance compares the likelihood under our estimated model to that under the saturated model where the value of the spectrum in each time block, scenario and frequency is assigned its own parameter. The deviances are largest at the edge of the maximum present-day sea ice extent in the Southern Ocean, and relatively homogeneous elsewhere. The relatively poorer fit at ice margins is expected, since variability decreases substantially here as sea ice retreats, and those changes are therefore based in part on absolute temperatures. Any statistical model based purely on changes in temperature, rather than absolute temperatures, will have difficulties capturing variability changes due to phase changes between ice and water. This result should serve as a warning against using such methods over locations, scenarios and time periods in which the response to $[CO_2]$ changes is highly nonlinear.

To address how well our statistical model is able to emulate GCM projected changes in variability for scenarios in some sense within the range spanned by our ensemble, we re-estimate our model using (a) all but the realizations under the medium scenario, and (b) only the realizations under the medium scenario. If the conclusions we draw from (a) match those drawn from (b), this is evidence

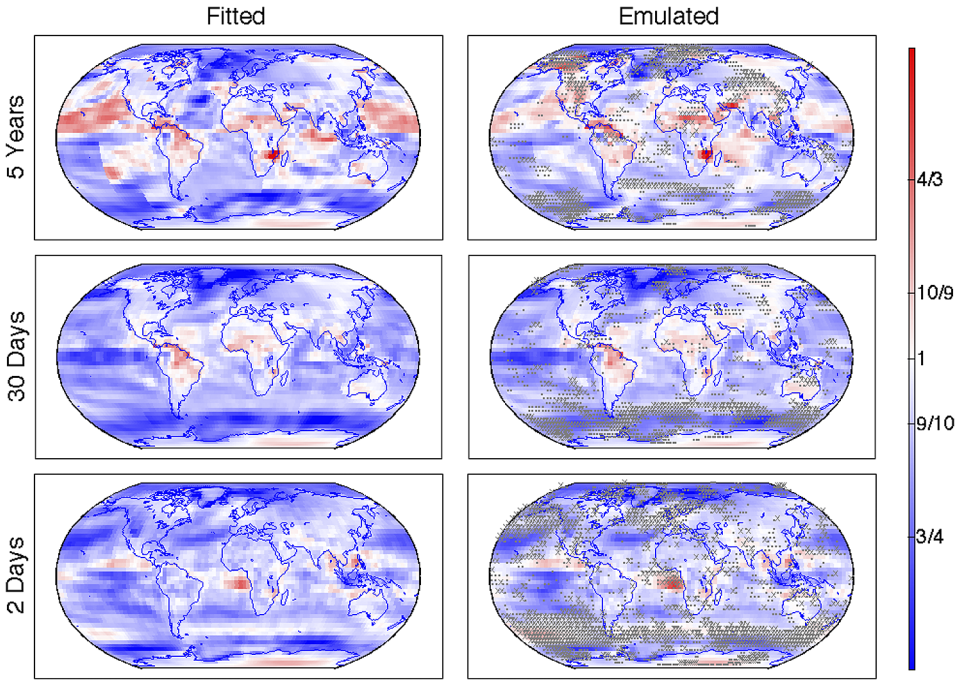

FIG. 6. *Estimates of changes in marginal spectra, at three frequencies, for the medium scenario at model year* 2100 *compared to the preindustrial climate. Left, estimates use only the medium scenario realizations. Right, estimates use all but the medium scenario realizations* (*i.e., are estimated as an emulator*). *Note that the apparent sudden change in behavior for low frequency variability in the Pacific Ocean* (*top left*) *is an artifact of the minimum bandwidth chosen for smoothing in these two adjacent regions*; *see Supplement* S2 [*Poppick et al.* (2016)] *for details on bandwidth selection. Locations are marked with "·" (or "x") when the difference between the emulator and the fitted model is more than two* (*or three*) *standard errors away from zero. The patterns are similar under both schemes, with most of the differences at locations where our model would not be expected to be a good description of changes in variability* (*e.g., at ice margins*).

that we have successfully emulated the changes in covariance structure under the medium scenario. We compare projected changes in marginal evolutionary spectra at year 2100 of the medium scenario, estimated under these two schemes (Figure 6). The estimated global patterns of changes in variability are quite similar under the two schemes. In an absolute sense, the biggest differences between the two schemes are at the lowest frequencies, but recall that since we have reason to believe that the ratios of spectra are less smooth at lower frequencies, we smooth with a smaller bandwidth at those frequencies and, therefore, our estimates of these changes are more uncertain. Globally, the differences between the estimates under schemes (a) and (b) are within two standard errors of zero in about 60–75% of the grid cells, depending on the frequency of interest. (Over land, the differences are within two standard errors in about 70–80% of the grid cells.) The locations

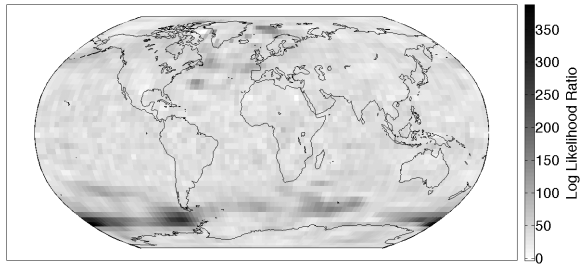

FIG. 7. *Log likelihood ratios comparing our proposed model to the reduced model taking* $\delta_{l1}(\omega) = 0$. *The models were estimated using all but the medium scenario realizations and the likelihoods were computed with just the medium scenario realizations, so the likelihood ratio is a comparison of the quality of emulation* (*no adjustment for model complexity is needed*). *In all but three locations on the globe, the likelihood under the full model is larger, which is an indication that for the purposes of emulation it is useful to include* $\delta_{l1}(\omega)$ *in the model.*

where there are significant differences between the two schemes are, unsurprisingly, often those where we have argued that the model should have trouble, such as in the Southern Ocean. In these locations, the emulator usually underestimates variability changes.

As discussed above, a feature of our model is that changes in variability depend not only on the change in regional mean temperature but also on the rate at which those changes occur. One might ask whether the simpler model that omits the second term [i.e., $\delta_{l1}(\omega) = 0$] is just as good at emulating changes in variability. Figure 7 displays the predictive log likelihood ratio comparing the simpler model to our proposed model; by predictive log likelihood, we mean that the models are estimated as emulators, excluding the medium scenario realizations, and the likelihoods are evaluated for the medium scenario realizations (as such, no adjustment for model complexity is necessary). At all but three out of the 4608 locations, the full model has a larger predictive likelihood than the simpler model, which indicates that for the purposes of emulation it is useful to allow for a nonzero term involving the rate of change of warming.

6. Discussion. In this work we describe a method for transforming observed temperatures to produce simulations of future temperatures when the climate is in a transient state, based on the projected changes in means and temporal covariances in GCM output. We believe this approach should yield more realistic simulations of future climate than do either GCM runs or simulations based on modifying GCM runs.

Any observation-driven procedure is of course limited by the observational record. Observations have some intrinsic uncertainty not explicitly accounted for in this work. As suggested in Section 1, it would be possible to explore the effect of these uncertainties on the resulting simulation by repeating the simulation

using different data products. Furthermore, the observational record is of a limited length and our procedure as described provides exactly one simulation of future temperatures equal in length to the observational record. As also suggested by Leeds, Moyer and Stein (2015), longer simulations could be produced either by recycling the observations entirely or by resampling them to generate new pseudo-observations.

An important feature of the procedure we describe is that our simulations preserve many features of the observational record not accounted for explicitly in the procedure. This paper is concerned with changes in only the temporal covariance structure of temperatures in transient climates. In the methodology described here, the simulation therefore preserves, for example, the spatial coherence spectra of the observations. While projected changes in spatial coherences in the model we study appear to be small (Section S5), changes in spatial coherences may also be important for societal impacts. We leave for future research the possibility of extending the methodology to account for such changes. This extension would be challenging and interesting, in part because temperatures are nonstationary in space with abrupt, local changes due to geographic effects.

Another challenging and interesting extension of our methods would be to jointly simulate future temperature and precipitation. Our work has focused on simulating temperatures, but potential changes in precipitation are also important for societal impacts. While there have been some model-driven proposals for jointly simulating temperature and precipitation [Piani and Haerter (2012), Vrac and Friederichs (2015)], to our knowledge, most approaches (both model- and observation-driven) proceed by simulating the two quantities separately. Versions of the simple Delta method can and are used for monthly precipitation, with the assumption that the GCM captures multiplicative (rather than additive) changes in rainfall amount [see, e.g., Teutschbein and Seibert (2012) and references therein for a review of common precipitation simulation methods]. A simple Delta method cannot, however, capture the changes on the timescale of individual rainfall events, whose intensity changes differently than that of time-averaged rainfall, with projections of less frequent but more intense storms [e.g., Trenberth (2011)]. Our approach, based on spectral methods, is likely also inadequate for characterizing changes in variability of daily precipitation, because daily precipitation often takes the value zero. (Data sources for daily local precipitation are also more problematic than those for temperatures, since reanalyses provide a poor reproduction of precipitation structure and interpolating sparse, complex precipitation fields is difficult.) More sophisticated observation-driven simulation methods for precipitation remain an area of research, as does the joint simulation of temperature and precipitation. In the context of this paper, where changes to the correlation structure of temperatures are detectable but not very large, we expect that separately simulating temperature and precipitation (as in common practice) will not result in large changes to their bivariate dependence structure.

Finally, the characterization of variability changes in transient climates is itself an issue of scientific interest. One of our motivations for developing the methods described here is to enable studying and ultimately comparing different GCM projections of changes in temperature variability. Most publicly available GCM runs (including most runs mandated by the IPCC) describe plausible future climates, which are necessarily in transient states. The statistical model we develop uses the GCM change in regional mean temperature and its rate of change to describe the GCM projected changes in covariance structure; in the GCM runs we study, these factors effectively summarize the projected changes in covariance. While we have investigated changes in variability in only one GCM, at relatively coarse resolution, we hope that our methods are applicable across GCMs, and may aid in carrying out a comparison across different GCMs in a coherent and interpretable way.

Acknowledgments. We thank William Leeds and Joseph Guinness for helpful discussions and for providing code related to their manuscripts. This work was completed in part with resources provided by the University of Chicago Research Computing Center.

SUPPLEMENTARY MATERIAL

Supplement A: Details on inference and computation, and additional figures (DOI: 10.1214/16-AOAS903SUPPA; .pdf). Additional details on estimating the mean changes in temperatures used in model (6) and the simulation (4); details on estimating the components δ_{l0} and δ_{l1} in model (6) and their associated standard errors; details on computing the proposed simulation; additional figures exploring the GCM projected variability changes and comparing the GCM output with the observational record; and a description of an animation of the proposed simulation.

Supplement B: Animation of global simulation (DOI: 10.1214/16-AOAS903SUPPB; .zip). An animation of the proposed simulation.

REFERENCES

BARNES, E. A. (2013). Revisiting the evidence linking Arctic amplification to extreme weather in midlatitudes. *Geophys. Res. Lett.* **40** 4734–4739.

BHAT, K. S., HARAN, M., OLSON, R. and KELLER, K. (2012). Inferring likelihoods and climate system characteristics from climate models and multiple tracers. *Environmetrics* **23** 345–362. MR2935569

CASTRUCCIO, S. and STEIN, M. L. (2013). Global space-time models for climate ensembles. *Ann. Appl. Stat.* **7** 1593–1611. MR3127960

CASTRUCCIO, S., MCINERNEY, D. J., STEIN, M. L., LIU CROUCH, F., JACOB, R. L. and MOYER, E. J. (2014). Statistical emulation of climate model projections based on precomputed GCM runs. *J. Climate* **27** 1829–1844.

CHANG, W., HARAN, M., OLSON, R. and KELLER, K. (2014). Fast dimension-reduced climate model calibration and the effect of data aggregation. *Ann. Appl. Stat.* **8** 649–673. MR3262529

COLLINS, W. D., BITZ, C. M., BLACKMON, M. L., BONAN, G. B., BRETHERTON, C. S., CARTON, J. A., CHANG, P., DONEY, S. C., HACK, J. J., HENDERSON, T. B. et al. (2006). The community climate system model version 3 (CCSM3). *J. Climate* **19** 2122–2143.

DAHLHAUS, R. (1997). Fitting time series models to nonstationary processes. *Ann. Statist.* **25** 1–37. MR1429916

DAHLHAUS, R. (2000). A likelihood approximation for locally stationary processes. *Ann. Statist.* **28** 1762–1794. MR1835040

DAHLHAUS, R. (2012). Locally stationary processes. In *Handbook of Statistics*, *Time Series Analysis*: *Methods and Applications* **30** 351–408. North-Holland, Amsterdam.

DECKER, M., BRUNKE, M. A., WANG, Z., SAKAGUCHI, K., ZENG, X. and BOSILOVICH, M. G. (2012). Evaluation of the reanalysis products from GSFC, NCEP, and ECMWF using flux tower observations. *J. Climate* **25** 1916–1944.

FRANCIS, J. A. and VAVRUS, S. J. (2012). Evidence linking Arctic amplification to extreme weather in mid-latitudes. *Geophys. Res. Lett.* **39** L06801.

GOTWAY, C. A. and YOUNG, L. J. (2002). Combining incompatible spatial data. *J. Amer. Statist. Assoc.* **97** 632–648. MR1951636

GUINNESS, J. and STEIN, M. L. (2013). Transformation to approximate independence for locally stationary Gaussian processes. *J. Time Series Anal.* **34** 574–590. MR3101381

HAWKINS, E., OSBORNE, T. M., HO, C. K. and CHALLINOR, A. J. (2013). Calibration and bias correction of climate projections for crop modelling: An idealised case study over Europe. *Agric. For. Meteorol.* **170** 19–31.

HO, C. K., STEPHENSON, D. B., COLLINS, M., FERRO, C. A. T. and BROWN, S. J. (2012). Calibration strategies: A source of additional uncertainty in climate change projections. *Bull. Am. Meteorol. Soc.* **93** 21–26.

HOLMES, C. R., WOOLLINGS, T., HAWKINS, E. and DE VRIES, H. (2015). Robust future changes in temperature variability under greenhouse gas forcing and the relationship with thermal advection. *J. Climate* **2015**.

IPCC (2001). *Climate Change* 2001: *The Scientific Basis. Contribution of Working Group I to the Third Assessment Report of the Intergovernmental Panel on Climate Change* (J. T. HOUGHTON, Y. DING, D. J. GRIGGS, M. NOGUER, P. J. VAN DER LINDEN, X. DAI, K. MASKELL and C. A. JOHNSON, eds.). Cambridge Univ. Press, New York.

IPCC (2007). *Climate Change* 2007: *The Physical Science Basis. Contribution of Working Group I to the Fourth Assessment Report of the Intergovernmental Panel on Climate Change* (S. SOLOMON, D. QIN, M. MANNING, Z. CHEN, M. MARQUIS, K. B. AVERYT, M. TIGNOR and H. L. MILLER, eds.). Cambridge Univ. Press, New York.

IPCC (2013). *Climate Change* 2013: *The Physical Science Basis. Contribution of Working Group I to the Fifth Assessment Report of the Intergovernmental Panel on Climate Change* (T. STOCKER, D. QIN, G.-K. PLATTNER, M. TIGNOR, S. K. ALLEN, J. BOSCHUNG, A. NAUELS, Y. XIA, V. BEX and P. M. MIDGLEY, eds.). Cambridge Univ. Press, New York.

LEEDS, W. B., MOYER, E. J. and STEIN, M. L. (2015). Simulation of future climate under changing temporal covariance structures. *Advances in Statistical Climatology Meteorology and Oceanography* **1** 1–14.

MORICE, C. P., KENNEDY, J. J., RAYNER, N. A. and JONES, P. D. (2012). Quantifying uncertainties in global and regional temperature change using an ensemble of observational estimates: The HadCRUT4 data set. *J. Geophys. Res.* **117**. D08101.

NEUMANN, M. H. and VON SACHS, R. (1997). Wavelet thresholding in anisotropic function classes and application to adaptive estimation of evolutionary spectra. *Ann. Statist.* **25** 38–76. MR1429917

OMBAO, H., RAZ, J., VON SACHS, R. and GUO, W. (2002). The SLEX model of a non-stationary random process. *Ann. Inst. Statist. Math.* **54** 171–200. MR1893549

PIANI, C. and HAERTER, J. O. (2012). Two dimensional bias correction of temperature and precipitation copulas in climate models. *Geophys. Res. Lett.* **39** L20401.

POPPICK, A., MCINERNEY, D. J., MOYER, E. J. and STEIN, M. L. (2016). Supplement to "Temperatures in transient climates: Improved methods for simulations with evolving temporal covariances." DOI:10.1214/16-AOAS903SUPP.

PRIESTLEY, M. B. (1981). *Spectral Analysis and Time Series. Vol.* 2. Academic Press, New York. MR0628736

ROUGIER, J., SEXTON, D. M., MURPHY, J. M. and STAINFORTH, D. (2009). Analyzing the climate sensitivity of the HadSM3 climate model using ensembles from different but related experiments. *J. Climate* **22** 3540–3557.

SAHA, S., MOORTHI, S., PAN, H.-L., WU, X., WANG, J., NADIGA, S., TRIPP, P., KISTLER, R., WOOLLEN, J., BEHRINGER, D. et al. (2010). The NCEP climate forecast system reanalysis. *Bull. Am. Meteorol. Soc.* **91** 1015–1057.

SALAZAR, E., SANSÓ, B., FINLEY, A. O., HAMMERLING, D., STEINSLAND, I., WANG, X. and DELAMATER, P. (2011). Comparing and blending regional climate model predictions for the American Southwest. *J. Agric. Biol. Environ. Stat.* **16** 586–605. MR2862300

SANSÓ, B. and FOREST, C. (2009). Statistical calibration of climate system properties. *J. R. Stat. Soc. Ser. C. Appl. Stat.* **58** 485–503. MR2750089

SANSÓ, B., FOREST, C. E. and ZANTEDESCHI, D. (2008). Inferring climate system properties using a computer model. *Bayesian Anal.* **3** 1–37. MR2383247

SANTER, B. D., WIGLEY, T. M. L., SCHLESINGER, M. E. and MITCHELL, J. F. B. (1990). *Developing Climate Scenarios from Equilibrium GCM Results*. Max-Planck-Institut für Meteorologie, Hamburg.

SCHNEIDER, T., BISCHOFF, T. and PŁOTKA, H. (2015). Physics of changes in synoptic midlatitude temperature variability. *J. Climate* **28** 2312–2331.

SCREEN, J. A. and SIMMONDS, I. (2013). Exploring links between Arctic amplification and midlatitude weather. *Geophys. Res. Lett.* **40** 959–964.

SEMENOV, M. A. and BARROW, E. M. (1997). Use of a stochastic weather generator in the development of climate change scenarios. *Clim. Change* **35** 397–414.

TEUTSCHBEIN, C. and SEIBERT, J. (2012). Bias correction of regional climate model simulations for hydrological climate-change impact studies: Review and evaluation of different methods. *J. Hydrol.* **456** 12–29.

TRENBERTH, K. E. (2011). Changes in precipitation with climate change. *Clim. Res.* **47** 123.

VRAC, M. and FRIEDERICHS, P. (2015). Multivariate—intervariable, spatial, and temporal—bias correction. *J. Climate* **28** 218–237.

WANG, W., XIE, P., YOO, S.-H., XUE, Y., KUMAR, A. and WU, X. (2011). An assessment of the surface climate in the NCEP climate forecast system reanalysis. *Clim. Dyn.* **37** 1601–1620.

WHEELER, T. R., CRAUFURD, P. Q., ELLIS, R. H., PORTER, J. R. and VARA PRASAD, P. V. (2000). Temperature variability and the yield of annual crops. *Agric. Ecosyst. Environ.* **82** 159–167.

WILKS, D. S. and WILBY, R. L. (1999). The weather generation game: A review of stochastic weather models. *Prog. Phys. Geogr.* **23** 329–357.

WILLIAMSON, D., GOLDSTEIN, M., ALLISON, L., BLAKER, A., CHALLENOR, P., JACKSON, L. and YAMAZAKI, K. (2013). History matching for exploring and reducing climate model parameter space using observations and a large perturbed physics ensemble. *Clim. Dyn.* **41** 1703–1729.

WOOD, A. W., LEUNG, L. R., SRIDHAR, V. and LETTENMAIER, D. P. (2004). Hydrologic implications of dynamical and statistical approaches to downscaling climate model outputs. *Clim. Change* **62** 189–216.

YEAGER, S. G., SHIELDS, C. A., LARGE, W. G. and HACK, J. J. (2006). The low-resolution CCSM3. *J. Climate* **19** 2545–2566.

A. POPPICK
M. L. STEIN
DEPARTMENT OF STATISTICS
UNIVERSITY OF CHICAGO
CHICAGO, ILLINOIS 60637
USA
E-MAIL: apoppick@galton.uchicago.edu
stein@galton.uchicago.edu

D. J. MCINERNEY
SCHOOL OF CIVIL, ENVIRONMENTAL
AND MINING ENGINEERING
UNIVERSITY OF ADELAIDE
ADELAIDE, SA 5005
AUSTRALIA
E-MAIL: david.mcinerney@adelaide.edu.au

E. J. MOYER
DEPARTMENT OF THE GEOPHYSICAL SCIENCES
UNIVERSITY OF CHICAGO
CHICAGO, ILLINOIS 60637
USA
E-MAIL: moyer@uchicago.edu